α, and MIP-1 in prompting the fever response associated with bacterial, viral, or parasitic infections as well as malignancies.

REFERENCES AND NOTES

1. E. Atkins, *Physiol. Rev.* **40**, 580 (1960).
2. C. A. Dinarello, J. G. Cannon, S. M. Wolff, *Rev. Infect. Dis.* **10**, 168 (1988).
3. C. A. Dinarello *et al.*, *J. Exp. Med.* **163**, 1433 (1986).
4. C. A. Dinarello *et al.*, *J. Clin. Invest.* **74**, 906 (1984).
5. S. D. Wolpe *et al.*, *J. Exp. Med.* **167**, 570 (1988).
6. G. Davatelis *et al.*, *ibid.*, p. 1939.
7. B. Sherry *et al.*, *ibid.*, in press.
8. F. Coceani, I. Bishai, J. Lees, S. Sirko, *Yale J. Biol. Med.* **59**, 169 (1986).
9. C. A. Dinarello, S. O. Marnoy, L. J. Rosenwasser, *J. Immunol.* **130**, 890 (1983).
10. J.-M. Dayer, B. Beutler, A. Cerami, *J. Exp. Med.* **162**, 2163 (1985).

11. Supported by the Swiss National Science Foundation (grant 3.400.0.86), by NIH grant AI121359, and a grant from Chiron Corporation. We thank C. A. Dinarello for criticism of the manuscript.

24 August 1988; accepted 12 December 1988

Block of Stretch-Activated Ion Channels in *Xenopus* Oocytes by Gadolinium and Calcium Ions

XIAN-CHENG YANG AND FREDERICK SACHS

Gadolinium ions produce three distinct kinds of block of the stretch-activated (SA) ion channels in *Xenopus* oocytes: a concentration-dependent reduction in channel open time, a concentration-dependent reduction in open channel current, and a unique, steeply concentration-dependent, reversible inhibition of channel opening. This last effect reduces the probability of a channel being open from about 10^{-1} at 5 μ*M* to less than 10^{-5} at 10 μ*M* gadolinium. Calcium has effects on open time and current similar to that of gadolinium, but this channel is permeable to calcium and calcium does not completely inhibit channel activity. The availability of a blocker for SA ion channels may help to define their physiological function, and will simplify the use of oocytes as an expression system for ion channels.

GADOLINIUM IS A TRIVALENT LANthanide with an ionic radius (0.938 Å) close to that of Na^+ (0.97 Å) and Ca^{2+} (0.99 Å) (*1*). Gadolinium (Gd^{3+}) blocks gravity sensing, but not growth, in the roots of plants (*2*), and since gravity sensing was hypothesized to depend on SA channels (*3*), we directly examined the effects of Gd^{3+} on SA channels. *Xenopus* oocytes have an endogenous, SA, nonselective cation channel (*4, 5*) which is blocked by 10 μ*M* Gd^{3+} applied extracellularly in outside-out patches (Fig. 1A) and in cell-attached patches (Fig. 2A). At 10 μ*M* Gd^{3+}, channel activity disappeared within 30 s. This could be demonstrated by making cell-attached patches with pipettes containing Gd^{3+} or by perfusing outside-out patches with Gd^{3+}. No recovery of activity was seen even when the stimulation was increased to 50 mmHg suction or when the pipette was held at a strong depolarizing potential for long periods in an attempt to draw Gd^{3+} out of the channel. The block, however, was reversible. Washout of Gd^{3+} was shown in outside-out patches (Fig. 1A) and cell-attached patches (legend to Fig. 1A). Gd^{3+} did not seem to affect the SA channel–gating mechanism directly, since the sensitivity to membrane tension was nearly independent of Gd^{3+} concentration (Fig. 2B).

Two other lanthanides, lanthanum and lutetium, with ionic radii of 1.061 Å and 0.85 Å, respectively (*1*), also blocked the oocyte SA channels, but only at concentrations greater than 100 μ*M*. At concentrations below 10 μ*M*, Gd^{3+} reduced the open channel current and the bursting kinetics of the channel became more "flickery" with shorter open times (Fig. 1A).

Because Gd^{3+} competes with Ca^{2+} during exocytosis in pituitary cells (*6*) and with Ca^{2+} binding to calmodulin (*7*), we also examined the effects of Ca^{2+} on oocyte SA channels. In contrast to Gd^{3+}, Ca^{2+} carries a significant amount of current through this channel (Fig. 1B). As with low concentrations of Gd^{3+} (below 10 μ*M*), the addition of Ca^{2+}- to Na^+-containing saline reduced the amplitude of the channel currents and caused the kinetics to become more flickery (Fig. 1B). Competition between Ca^{2+} and Na^+ also occurs in SA channels in lens epithelia from the frog (*8*).

The reduction in channel open time by Gd^{3+} and Ca^{2+} have a number of similarities. For both ions at all concentrations, the mean open time was independent of pressure and voltage (Fig. 3, A and B), suggesting that any barriers to binding lay outside the membrane field. The difference between Ca^{2+} and Gd^{3+} is that the reduction of open time by Ca^{2+} saturates at a finite value, whereas the reduction by Gd^{3+} does not, at least not within the tested concentration range (Fig. 3C).

The blocking kinetics were analyzed according to the traditional closed-open-block kinetic model (*9*). The block by Gd^{3+} follows one prediction of this model—the reciprocal of the open time is a linear function of the blocking ion concentration (Fig. 3C). The blocking rate constant extracted from fitting the data in Fig. 2C is $1.6 \times 10^8 M^{-1}$ s^{-1}, indicating a binding reaction that is nearly diffusion-controlled (*10*). The lack of

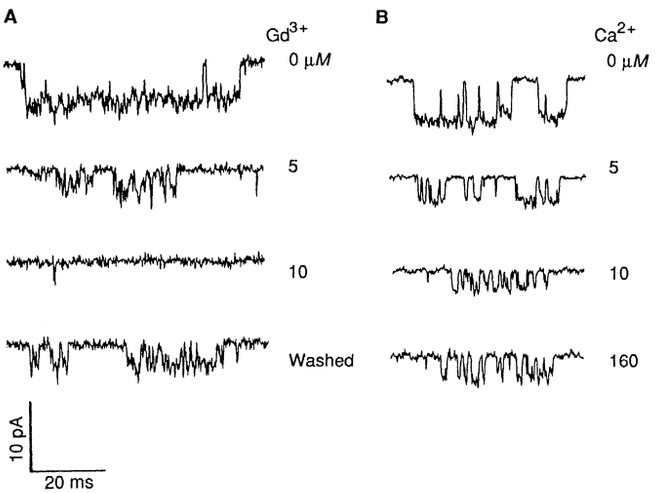

Fig. 1. (**A**) Effect of Gd^{3+} on single-channel currents recorded from an outside-out patch (pipette potential of −70 mV). Gadolinium at 10 μ*M* blocks SA channel activity reversibly (5 outside-out patches and 16 cell-attached patches). Gadolinium at 5 μ*M* reduces both channel open time and amplitude. The downward currents indicate flow from bath to pipette. The washout of Gd^{3+} is observed also in cell-attached patches by pretreating the cells with 10 μ*M* Gd^{3+} for 30 min or longer and then patching with pipettes containing Gd^{3+}-free Na^+ saline. (**B**) Single-channel current recorded from cell-attached patches exposed to Ca^{2+} (membrane potential of −100 mV). The bottom trace in (B), with a vertical scale of 5pA (rather than 10 pA), is a Ca^{2+} current through SA channels (160 m*M* $CaCl_2$ and 0 m*M* Na^+, buffered with 10 m*M* Hepes–tetraethylammonium hydroxide, *p*H 7.4). Preparation of oocytes (*3, 17*) and recording techniques (*28*) followed published procedures. Pipette solutions were 150 m*M* NaCl, 10 m*M* Hepes-NaOH, and $GdCl_3$ or $CaCl_2$ as indicated in the figure, *p*H 7.4. Bath solution was frog normal saline: 115 m*M* NaCl, 2 m*M* KCl, 1.8 m*M* $CaCl_2$, and 10 m*M* Hepes-NaOH, *p*H 7.4 (18° to 23°C).

Biophysical Sciences, 105 Parker Hall, State University of New York, Buffalo, NY 14214.

voltage dependence for the blocking rate constant suggests that Gd^{3+} blocks the channel outside the membrane electric field.

The unblocking rate for Gd^{3+} could not be reliably measured in these experiments. In contrast to the open channel block observed with weakly bound local anesthetics, in which bursts get longer and the unblocking rate can be easily estimated (*9*), with Gd^{3+} (and Ca^{2+}) the bursts get shorter (Fig. 1) because the residence time of the blocker is sufficiently long that the bursts seem to end. Because there are few long closed periods, the uncertainty in the distribution is high, and changes produced by the blockage are difficult to determine.

In contrast to the results obtained with Gd^{3+} in which the open time appeared to approach zero with increasing concentration, the open time obtained with Ca^{2+} reached a finite minimum (Fig. 3C). The apparent half-block concentration (K_d) for Ca^{2+} was 0.33 m*M* and the extrapolated open time at infinite Ca^{2+} (legend to Fig. 2) was 0.48 ms—the value observed with 160 m*M* Ca^{2+} (Na^+-free). The open time decreased from 2.9 ms with pure Na^{2+} to 0.48 ms with pure Ca^{2+}. This leveling off of the open time is not explained by first-order kinetics. A simple alternative explanation is that Ca^{2+} is not plugging the channel but rather is binding to an allosteric site that lowers the energy barrier between the open state and an adjacent closed state. This is equivalent to having two open states, Ca^{2+} liganded or unliganded. We could find no evidence of a new, Ca^{2+}-dependent, open time. Perhaps there is a rapid exchange between the liganded and unliganded forms (relative to the open time) so that we only resolve a single lifetime. Such allosteric changes associated with Ca^{2+} binding have been reported for L-type Ca^{2+} channels (*11*). The lack of voltage-dependence for the reduction in open time by Ca^{2+} suggests that the allosteric site is outside the membrane electric field and that the site is not distorted by any movement of the channel in the field due to structural dipoles. The apparent open channel block by Gd^{3+} could involve the same allosteric site, but because of the restricted concentration range (less than 10 μ*M*), we could not observe the saturation of open time with concentration.

In addition to shortening the open time, Gd^{3+} and Ca^{2+} both decrease the channel current over the entire voltage range from −30 mV to −200 mV (Fig. 4, A and B). The normal current-voltage (*I-V*) curve for Na^+ and other alkali cations is inwardly rectifying (*4*) and can be described by a two-barrier one-site (2B1S) permeation model (*13*). However, the *I-V* curve with pure Ca^{2+} (Na^+-free) is almost linear with a slope conductance of 20 pS, nearly identical to the values reported for other SA channels (*8, 13, 14*). Gadolinium shifts the *I-V* curves to the left along the voltage axis (a 26-mV shift in voltage at 5 μ*M* Gd^{3+}) without changing

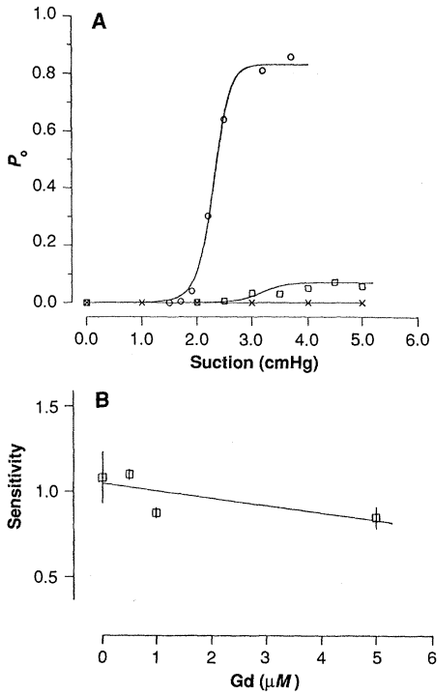

Fig. 2. (**A**) P_o as functions of suction and Gd^{3+} concentration. A nonlinear, least-square algorithm was used for curve fitting (*29*). The solid lines represent the best fit to a Boltzmann distribution (*30, 31*):

$$P_o = P_{max}/[1 + K \exp(-\vartheta p^2)] \quad (1)$$

where P_{max} is the maximum probability of channel being open, K is the equilibrium constant at zero pressure, and ϑ is the sensitivity to membrane tension, which determines the slope of the activation curve. The free energy for gating is proportional to the square of membrane tension. Tension is linearly related to pressure, p, by Laplace's law. (**B**) The sensitivity to membrane tension as a function (ϑ) of Gd^{3+}. ϑ is extracted by fitting the data to Eq. 1. Each point is the mean from three experiments.

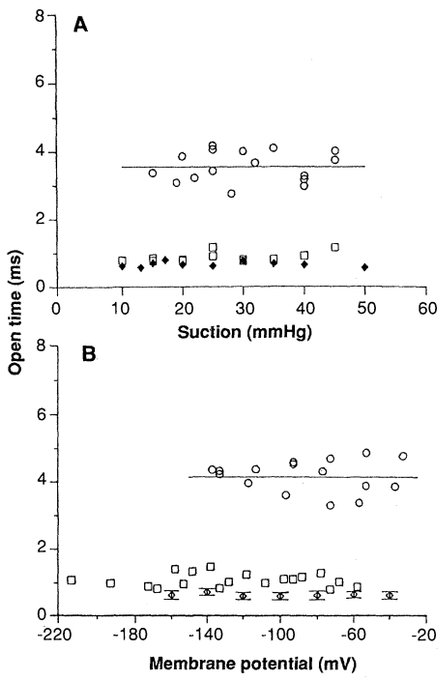

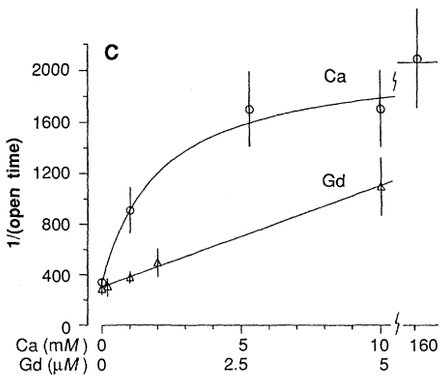

Fig. 3. (**A** and **B**) The mean open time of SA channel is independent of both suction and voltage at each concentration of Gd^{3+} or Ca^{2+}. All data in this figure are obtained from cell-attached patches. The solid lines parallel to abscissas represent the arithmetic mean of all data points for experiments done with Na^+ saline. The most scattered points are within ±1 ms (or 20%) of the mean. Each data point is the time constant derived from fitting the open time histogram. The confidence limits (90%) for each data point are within 33% of the mean. ○, Na^+ only; □, 5 μ*M* Gd^{3+}; ◆, 5.3 m*M* Ca^{2+}. (A) Na^+, $n = 4$; Gd^{3+}, $n = 3$; Ca^{2+}, $n = 1$. (B) Na^+, $n = 3$; Gd^{3+}, $n = 3$; Ca^{2+}, $n = 6$. (**C**) The reciprocal of mean open time as function of blocking ion concentration. Each point is the mean of the open time determined from 9 to 35 individual open time histograms. The straight line for Gd^{3+} has a slope of $1.6 \times 10^8 M^{-1}\ s^{-1}$ and an intercept of 304 s^{-1}. The Ca^{2+} data are fitted to a saturating function with an offset:

$$\tau_{open} = (\tau_m)\ (x_b + r)/(x_b + K_d) \quad (2)$$

where x_b is the blocker concentration; K_d is the half-block concentration; τ_m is open for pure Ca^{2+}; and the offset, r, is proportional to K_d. For the Ca^{2+} data, nonlinear regression yielded values of $\tau_m = 0.48$ ms, $K_d = 0.34$ m*M*, and $r = 2$ m*M*. The data were recorded with a bandwidth of DC-5 kHz on analog tape, filtered on playback at 2.5 kHz for Gd^{3+} and 5 kHz for Ca^{2+}, and digitized at 10 kHz and 20 kHz, respectively. An automated single-channel data analysis program (IPROC, AXON Instruments), was used for single-channel event detection and histogram construction (*32*). LPROC (Axon Instruments), a computer program for classifying and sorting single-channel data (*33*), was used for generating additional duration histograms. The open time histograms were generally fit with a single exponential function. A sum of two exponential functions was required for some histograms, and only the larger time constant was used for further analysis. We made a first order correction for missing events (*32, 34*), which yielded values that were 0.8 to 0.9 times shorter than the uncorrected values.

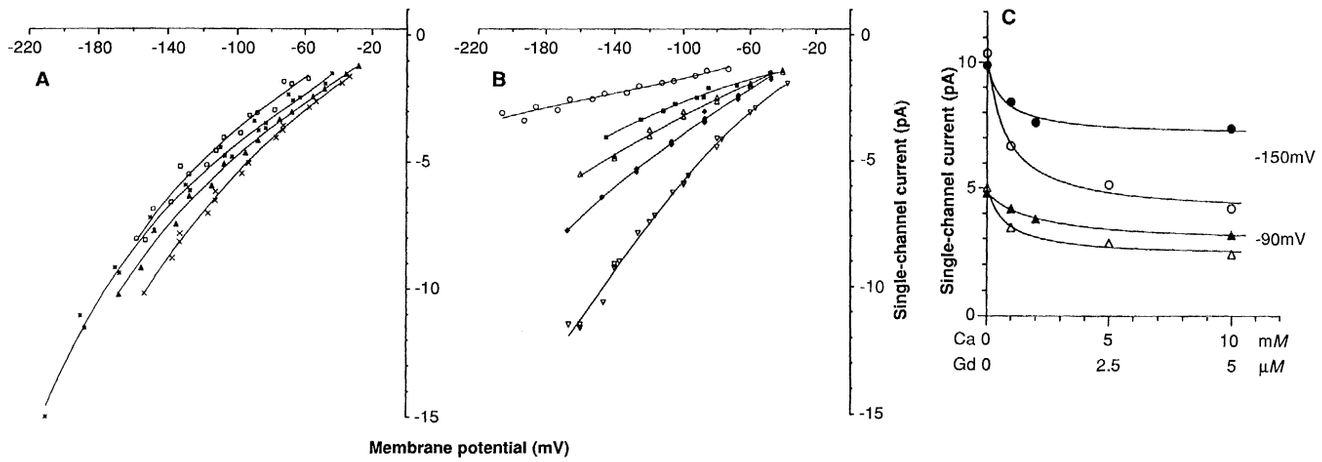

Fig. 4. (**A** and **B**) Single-channel *I-V* curves with blocking ions obtained from cell-attached patches. A symmetrical 2B1S permeation model was used for fitting the *I-V* curves (*35*). Each solid line represents the best fit to the 2B1S model through all the data points for each given experimental condition. The free energy values for calculation of the best fit lines (*35*) were G1 = 10.0 kT, G2 = 11.5 kT, and W = 0.59 kT for Na^+, and G1 = 12.4 kT, G2 = 8.9 kT, and W = 6.7 kT for Ca^{2+} (where G1 and G2 are peak heights for two barriers, and W is well depth for the site; the values of G1, and G2, and W are all relative to the free energy of aqueous solution outside the channel). The site is an electric distance of 0.25 from external side of the channel. (A) Gd^{3+} at 0 μ*M* (x; n = 3), 0.5 μ*M* (▲; n = 2), 1 μ*M* (■; n = 3), and 5 μ*M* (□; n = 3). (B) Ca^{2+} at 0 m*M* (▽; n = 4), 1 m*M* (◆; n = 4), 5 m*M* (△; n = 3), 10 m*M* (■; n = 3), and 160 m*M* (○; n = 2). (**C**) Single-channel currents as a function of blocking ion concentration derived from Fig. 4, A and B. ● and ▲, Gd^{3+}; ○ and △, Ca^{2+}.

the slope conductance. This suggests that the reduction in channel current produced by Gd^{3+} results from neutralization of negative surface charge, probably in the vestibule of the channel. This reduction in surface charge would decrease the local concentration of the highly permeant monovalent cations (*15*). In contrast to Gd^{3+}, the reduction of channel current produced by Ca^{2+} results from not only shifting the *I-V* curves along the voltage axis but also from reducing the slope conductance. The change in slope conductance reflects the stronger binding of Ca^{2+} [with a well depth of −6.7 kT (where k is Boltzmann's constant and T is absolute temperature)] over Na^+ (with a well depth of 0.59 kT) at the intrachannel site (legend to Fig. 4). Strong binding to this site reduces the exit rate, which determines the slope of the *I-V* curve. The difference in reduction of channel current by Gd^{3+} and Ca^{2+} results from the differences in the permeability of the channel to these two ions and their charges. Gadolinium seems to be impermeant, whereas Ca^{2+} is highly permeant. Because of its trivalent charge, Gd^{3+} is about 100-fold more effective than Ca^{2+} in screening negative surface charges (Fig. 4, A and B).

Gadolinium produces a complete inhibition of channel activity at 10 μ*M*. If that inhibition were caused by open channel block, the open time would be negligible at 10 μ*M*. By extrapolating the linear plot of the blocking rate as a function of concentration (Fig. 3C) to 10 μ*M*, the predicted open time is 0.53 ms, much too long to account for the "zero" probability of the channel being open. Similarly, the reduction of channel current by Gd^{3+} saturates to a non-zero minimum (Fig. 4C) and cannot explain the lack of activity. Thus, Gd^{3+} must also be capable of introducing another, and much longer lived, blocked state that has a lifetime greater than the duration of the experiment (about 300 s).

In more than 20 experiments, we found that channel activity persisted at 5 μ*M* Gd^{3+} (maximum probability of the channel being open, P_o, about 10^{-1}), but was unmeasurable at 10 μ*M* Gd^{3+} (maximum P_o less than 10^{-5}). Such a steep concentration dependence suggests a Hill coefficient that is greater than 7. Perhaps a cooperative transition takes place in the channel when a sufficient number of negatively charged sites are occupied by Gd^{3+}.

The results obtained with Ca^{2+} show that SA channels can serve as an independent pathway for transporting a significant amount of Ca^{2+} into cells. We estimate that in a mixture of 150 m*M* Na^+ and 1 m*M* Ca^{2+}, the current carried by Ca^{2+} through a single SA channel is about 0.01 to 0.1 pA at −60 mV (Fig. 4B). This current is comparable to that carried by single Ca^{2+} channels in normal saline (*16*). The density of SA channels ranges from 0.3 to 2 per square micrometer (*4, 17–19*), whereas the Ca^{2+}-channel density ranges from 0.1 per square micrometer in 3T3 fibroblasts (*20*) to 30 to 60 per square micrometer in snail neurons (*21*). Thus, SA channels may represent a substantial fraction of the cell's Ca^{2+} permeability. In fact, because SA channels are voltage dependent and opening with depolarization (*22*), SA channel currents could be mistaken for traditional, voltage-dependent, Ca^{2+} channel currents.

How specific is Gd^{3+} for oocyte SA channels relative to other channels? The SA channels in cultured *Xenopus* myocytes (nonselective cation channels) were blocked at the same concentration as in oocytes. The K^+-selective SA channels in rat astrocytes were not affected by 10 μ*M* Gd^{3+} (*23*). The SA channels in yeast (*24*), which are nonselective among cations and mildly selective for cations over anions, are blocked by Gd^{3+} at 10 μ*M* (*25*), in accordance with our observations. In T lymphocytes, 10 μ*M* Gd^{3+} does not block the delayed rectifier K^+ channel, although it does block volume regulation (*26*). In neuroblastoma-glioma hybrid cells, Gd^{3+} blocks only one component of whole-cell Ca^{2+} current, possibly that through the N-type Ca^{2+} channel (*27*). Gadolinium is not a generic channel blocker, and is the most potent blocker known for mechanoreceptive transducers. Gadolinium may also prove useful to those using *Xenopus* oocytes as an RNA expression system for ion channels.

REFERENCES AND NOTES

1. R. C. Weast, Ed., *CRC Handbook of Chemistry and Physics* (CRC Press, Boca Raton, FL, 1986).
2. B. Pickard, *Biophys. J.* **53**, 155a (1988).
3. K. L. Edwards and B. G. Pickard, *The Cell Surface in Signal Transduction*, E. Wagner, H. Greppin, B. Millet, Eds. (Springer-Verlag, Berlin, 1987), pp. 41–66.
4. B. Sakmann *et al.*, *Nature* **318**, 538 (1985).
5. X. C. Yang and F. Sachs, *Biophys. J.* **51**, 252a (1987).
6. E. Muscholl, K. Racke, A. Traut, *J. Physiol. (London)* **367**, 419 (1985).
7. J. M. Buccigross, C. L. O'Donnell, D. J. Nelson, *Biochem. J.* **235**, 677 (1986).
8. K. E. Cooper *et al.*, *J. Membrane Biol.* **93**, 259 (1986).
9. E. Neher and J. H. Steinbach, *J. Physiol. (London)* **277**, 153 (1978).
10. We were unable to find a reference for the diffusion coefficient of Gd^{3+} but it should be close to that of lanthanum, 1.105×10^{-5} cm^2 s^{-1} (*1*).

11. D. Pietrobon, B. Prod'hom, P. Hess, *Nature* **333**, 373 (1988).
12. X. C. Yang and F. Sachs, *Biophys. J.* **53**, 412a (1988).
13. J. B. Lansman, T. Hallam, T. J. Rink, *Nature* **325**, 811 (1987).
14. M. T. Kirber, J. J. Singer, J. V. Walsh, *Biophys. J.* **51**, 252a (1987).
15. J. A. Dani, *ibid.* **49**, 607 (1986).
16. R. W. Tsien, P. Hess, E. W. McCleskey, R. L. Rosenberg, *Annu. Rev. Biophys. Biophys. Chem.* **16**, 265 (1988).
17. C. Methfessel *et al.*, *Pfluegers Arch.* **407**, 577 (1986).
18. M. T. Kirber, J. V. Walsh, Jr., J. J. Singer, *Biophys. J.* **53**, 411a (1988).
19. W. J. Sigurdson, C. E. Morris, B. L. Brezden, D. R. Gardner, *J. Exp. Biol.* **127**, 191 (1987).
20. C. Chen, M. J. Corbley, T. M. Roberts, P. Hess, *Science* **239**, 1024 (1988).
21. O. A. Krishtal, V. I. Pidoplichko, Y. A. Shakhovalov, *J. Physiol. (London)* **310**, 423 (1981).
22. F. Guharay and F. Sachs, *ibid.* **353**, 119 (1985).
23. J. P. Ding, personal communication.
24. M. C. Gustin, X.-L. Zhou, B. Martinac, M. R. Culbertson, C. Kung, *Biophys. J.* **51**, 251a (1987).
25. M. C. Gustin, X.-L. Zhou, B. Martinac, C. Kung, *Science* **242**, 762 (1988).
26. C. Deutsch and S. C. Lee, *Renal Physiol.*, in press.
27. R. J. Docherty, *J. Physiol. (London)* **398**, 33 (1988).
28. O. P. Hamill, A. Marty, E. Neher, B. Sakmann, F. J. Sigworth, *Pfluegers Arch.* **391**, 85 (1981).
29. A. Auerbach and F. Sachs, *Biophys. J.* **45**, 187 (1984).
30. F. Guharay and F. Sachs, *J. Physiol. (London)* **352**, 685 (1984).
31. F. Sachs, *Membrane Biochem.* **6**, 173 (1986).
32. ———, J. Neil, N. Barkakati, *Pfluegers Arch.* **395**, 331 (1982).
33. Z. Xiang, J. Neil, A. Auerbach, *P. R. Health Sci. J.* **7** (2), 77 (1988).
34. E. Neher, *J. Physiol. (London)* **339**, 663 (1983).
35. B. Hille, *Ionic Channels of Excitable Membranes* (Sinauer, Sunderland, MA, 1984).
36. We thank J. P. Ding for providing unpublished results. A preliminary report on these results was presented at the 1988 Biophysical Society Meeting (*12*). Supported by the Muscular Dystrophy Association, USARO 22560-LS, NIH DK-37792, and the Health-care Instruments and Devices Institute at the State University of New York at Buffalo.

4 August 1988; accepted 2 December 1988

Neuroanatomical Correlates of Anticipatory Anxiety

ERIC M. REIMAN, MAUREEN J. FUSSELMAN, PETER T. FOX, MARCUS E. RAICHLE

Positron emission tomographic measurements of regional blood flow, a marker of local neuronal activity, were used to investigate the neuroanatomical correlates of a normal emotion. Healthy volunteers were studied before, during, and after anticipation of a painful electric shock. During anticipatory anxiety, there were significant blood flow increases in bilateral temporal poles, the same regions recently implicated in a lactate-induced anxiety attack in patients with panic disorder. Thus, the temporal poles seem to be involved in normal and pathological forms of human anxiety.

IN ORDER TO ESTABLISH THE NEUROBIology of an emotional response, researchers must be able to relate that response to the local processes of the living human brain. Previously, we used positron emission tomography (PET) to investigate the neuroanatomical correlates of panic disorder, a pathological form of human anxiety (*1–3*). Patients with panic disorder and normal control subjects were studied before and during lactate infusion, a procedure that precipitated an anxiety attack in many of the patients and none of the controls (*2, 3*). During the nonpanic state before the infusion, the patients who were vulnerable to lactate-induced panic had an abnormal asymmetry (left less than right) of blood flow, of blood volume, and of the metabolic rate for oxygen in the vicinity of Economo's region TH in the parahippocampal gyrus (*2*). During a lactate-induced anxiety attack, there were significant blood flow increases in bilateral regions of the temporal poles (*3*).

In the study reported here, we used PET measurements of regional blood flow, a marker of local neuronal activity (*4*), to investigate the neuroanatomical correlates of a normal form of human anxiety, that due to the anticipation of an external danger. Regional blood flow was measured in eight healthy volunteers (*5*) before, during, and after anticipation of a painful electric shock. These measurements were made with the PETT VI system, [^{15}O]H_2O, 40-s data acquisition periods, and an interscan duration of 10 min (*6, 7*). The subjects were informed that no shock would be delivered during the first and third measurements, but that a painful electric shock would be delivered sometime within a 2-min period after the second tracer administration; they were also informed that the severity of the shock was likely to increase with the passage of time before its arrival. A brief electric shock was delivered immediately after the second data acquisition period to maintain the credibility of the investigators for the remainder of the study; the severity of the stimulus was predetermined by its ability to produce mild discomfort in the investigators themselves (*8*).

The first scanning procedure permitted acclimation to the PET routine and provided data for post hoc comparisons. The second scanning procedure provided data corresponding to a state of anticipatory anxiety. The third scanning procedure provided baseline data for measuring the changes in

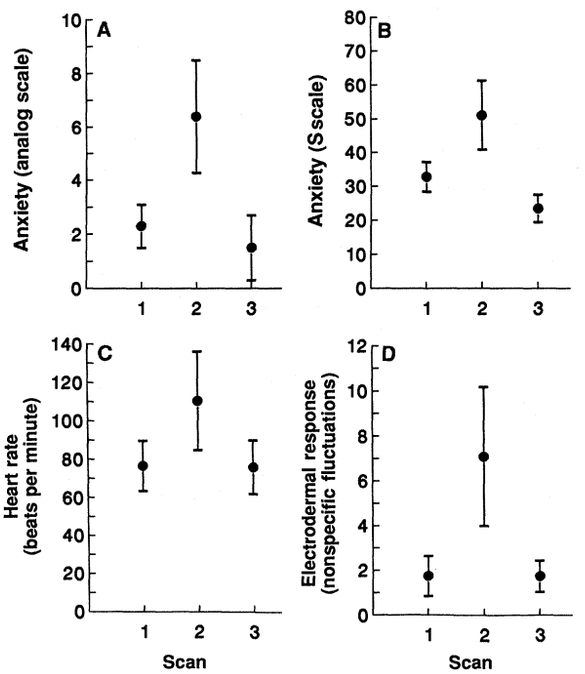

Fig. 1. Subjective and physiologic measurements of anxiety before (scan 1), during (scan 2), and after (scan 3) anticipation of a painful electric shock. Means and standard deviations are depicted for (**A**) the rating on an analog scale of anxiety, (**B**) the score on the S-Anxiety scale of the STAI (*10*), (**C**) heart rate, and (**D**) the number of nonspecific fluctuations in skin conductance. Scan 2 was distinguished from scans 1 and 3 by significant increases in all measures of anxiety (paired t tests, $P < 0.05$, Bonferroni correction for multiple comparisons).

E. M. Reiman, Department of Psychiatry and McDonnell Center for Studies of Higher Brain Function, Washington University School of Medicine, St. Louis, MO 63110.
M. J. Fusselman, Departments of Psychiatry and Neurology and Neurological Surgery, Washington University School of Medicine, St. Louis, MO 63110.
P. T. Fox, Mallinckrodt Institute of Radiology and Department of Neurology and Neurological Surgery, Washington University School of Medicine, St. Louis, MO 63110.
M. E. Raichle, Mallinckrodt Institute of Radiology, Department of Neurology and Neurological Surgery, and McDonnell Center for Studies of Higher Brain Function, Washington University School of Medicine, St. Louis, MO 63110.